Adaptive current-flow models of ECT: Explaining individual static impedance, dynamic impedance, and brain current delivery

Gozde Unal[1], Jaiti K. Swami[1], Carliza Canela[1], Samantha Cohen[2], Niranjan Khadka[3], Mohammad Rad[1], Baron Short[4], Miklos Argyelan[5], Harold Sackeim[6], Marom Bikson[1]

[1]Department of Biomedical Engineering, The City College of New York, CUNY, New York, NY

[2]Department of Biomedical Engineering, Cornell University, Ithaca, New York, 14850, USA,
[3]Department of Psychiatry, Laboratory for Neuropsychiatry and Neuromodulation, Massachusetts General Hospital, Harvard Medical School, MA, USA
[4]Department of Psychiatry and Behavioral Sciences, Medical University of South Carolina, Charleston, South Carolina, USA
[5]Center for Neurosciences, The Feinstein Institute for Medical Research, North Shore- Long Island Jewish Health System, Manhasset, New York, 11030, USA
[6]Department of Psychiatry and Radiology, Columbia University, New York, USA

Correspondence
Marom Bikson
Tel: (212) 650- 7076
email: bikson@ccny.cuny.edu

Gozde Unal
Tel: (212) 650- 7076
email: gozdeunal33@gmail.com

Conflict of Interest
The City University of New York (CUNY) has IP on neuro-stimulation systems and methods with authors NK and MB as inventors. MB has equity in Soterix Medical. MB served on the advisory boards, received grants, and/or consulted for Boston Scientific, Mecta, Halo Neuroscience, and GlaxoSmithKline Inc.

Abstract:

The physical properties of the Electroconvulsive Therapy (ECT) stimulus markedly effect both efficacy and cognitive side effects. Combining records of clinical ECT, device measurements, and MRI-derived FEM computational head models, we consider the sources and relationship between static impedance, dynamic impedance, and current delivered to the brain. To this end, we develop the first adaptive models of transcranial Electrical Stimulation, where local tissue conductivity is modulated by electric field. The models predict subject-specific static impedance and dynamic impedance, provide insight into their relationship, and predicts how ECT shapes tissue conductance and so how current reaches the brain.

Introduction

Ongoing advancements in the efficacy or specificity (reduced adverse effects) of Electroconvulsive therapy (ECT) rely on refinement in dose; namely electrode montage and stimulation waveform [1,2]. Dose optimization has followed heuristic approaches, and controversies remain unreconciled despite decades of research [3,4]. While static impedance and dynamic impedance has long been recognized as markers of individual difference, their etiology and consequence are undetermined [5] – including how they impact seizure generation [6–9].

For a given ECT dose, the pattern of current delivery to the brain is determined by individual anatomy and electric conductivity of each tissue layer (e.g. skin, skull) [10–12]. The finding that dynamic impedance is lower than static impedance is consistent with an increase in tissue conductivity in response to high (dynamic) verse low (static) current intensity. But it is unclear which tissue layers are responsible for this impedance difference, how current flow to the brain then altered, and with what implications to seizure genesis?

We developed the first individualized (MRI-derived) finite element method (FEM) simulations of electrical stimulation that incorporate changes in tissue resistivity by local current flow. These models explain the source of individual difference in static and dynamic impedance, how they relate, and how they impact seizure threshold.

Methods

Electrode preparation on static impedance: controlled experiments in healthy subjects

We conducted a pilot study to evaluate the role of electrode preparation (Thymapad, Somatics, Venice, Fl) on static impedance using healthy subjects (n=3) where six electrode preparation techniques could be compared. 1) Skin cleaning with saline and with Pretac (Pharmaceutical Innovations, Newark, New Jersey); 2) Alcohol (99%) skin cleaning with Pretac; 3) Skin cleaning with saline and with Pretac but 50% electrode contact area (achieved with using a plastic insulative sheet with a 2.5x2.5 cm annulus); 4) Alcohol cleaning only; 5) Skin cleaning with saline and with PVP-K90 1% (w/v) (Sigma-Aldrich Inch, St. Louis, Missouri); 6) Skin cleaning with saline and with PVP-K90 plus KCL (0.0003%). Pretac or PVP-K90 was applied to the electrode surfaces (300-500 uL) before placement. Electrodes were placed according to bifrontal placement instructions, avoiding hairline, with careful attention to ensure complete electrode-skin contact. Static impedance was measured using both a Spectrum 5000Q (Mecta, Tualatin, Oregon) and Thymatron System IV (Somatics), immediately after electrode application (t=0) and every minute for 17 minutes or until a stable impedance was recorded. Each subject and electrode preparation combination were tested 3 times, tests separated by >1 day.

RUL and BL Clinical ECT Data Set

Anonymized data was re-analyzed from a single-center ECT trial using right unilateral (RUL) and bilateral (BL). Only stimulation at 900 mA was included in our analysis. Except for the pulse width manipulation, stimulation waveform was identical in the ultrabrief and brief pulse groups. Ninety depressed patients were randomly assigned across four ECT groups: RUL ECT or BL

ECT, using either a traditional brief pulse (1.5 ms) or an ultrabrief pulse (0.3 ms). Seizure threshold was quantified at the first and last treatments using a titration procedure. At all other treatments (treatment sessions) electrical dosage was 2.5 or 6.0 times the seizure threshold at the first titration session for BL ECT and RUL ECT, respectively. The precision of seizure threshold is limited by resolution of titration steps and "floor effects" [8]. Still, the increase of seizure threshold with decreasing dynamic impedance is relatively established [8,9] for RUL and BL montages.

BF Clinical ECT Data Set

Anonymized data was re-analyzed from a single-center ECT trial series using BF ECT.

General modeling approach

Skin impedance decreases with increasing electrical current density, to a skin-specific asymptote of ~0.1-0.5 S/m at ~1 mA/cm^2. ECT electrode current density (current by electrode area) is >30 mA/cm^2. Overall head impedance decreases with increasing ECT intensity, to a subject-specific asymptote of ~200 Ohm at <800 mA and <200 V [5,13]. At low currents, minimum skin resistivity varies substantially with tested-conditions and across microscopic layers: spanning ~1x10^{-5} S/m for epidermal stratum corneum and ~2x10^{-4} to 0.2 S/m for layers of dermis and fat [14,15]. This range can be contrasted with skull conductivity of ~0.01 S/m.

It is intractable to model <0.1 mm tissue layers at full head-scale, necessitating approximation [16]. Adjacent tissue layers with mismatched resistivity can especially impact current flow patterns [17,18]. Given the above, we consider two scalp layers, "superficial-scalp" layer and "deep-scalp" layer, with superficial scalp minimally conductivity at low current (conditions of static impedance) and highly conductive at high current (conditions of dynamic impedance).

The capacitive properties (reactance) of tissue, notably skin layers, decrease at either high current [19] or at high frequency. Indeed, the notion that low-intensity (sub-perception) high-frequency (>7 kHz) current can be used before to estimate subject resistance for ECT dates to at least 1942 [20], and is reflected in contemporary use of high-frequencies to test static impedance. Therefore, we do not model tissue permittivity (reactance). We do represent the non-linear changes in resistivity to current flow.

Subject head segmentation and subject-generic tissue parameterization

High resolution T1-weighted anatomical MRIs were deidentified from a cohort of subjects (n=17) receiving clinical ECT at the Zucker Hillside Hospital. Each subject received 6-10 ECT sessions with electrodes configured in a bifrontal montage (with Pretac preparation). Of the seventeen subjects in this cohort, high resolution MRI-derived head models were constructed for four subjects (#21908, #22615, #22035, #21778) that were selected based on a range and variance in static and dynamic impedance values.

An automated segmentation pipeline based on algorithms in SPM8 [21] and updated for volume conduction models [22] was used to create initial image masks of scalp, skull, air,

meninges/cerebrospinal fluid, gray matter and white matter. Additional manual segmentation was applied to correct for noise, aliasing artifacts, and to separate superficial scalp and deep scalp layers. Unless otherwise indicated, segmented tissues were assigned fixed electrical conductivity[16]: skull (σ = 0.01 S/m), gray matter (σ = 0.276 S/m), white matter (σ = 0.126 S/m), meninges/cerebrospinal fluid (σ = 0.85 S/m), and air ($\sigma = 1e^{-15}$ S/m).

Deep-scalp layer was assigned a subject specific conductivity (σ_{DS}) between $4.5e^{-4}$ S/m and 0.008 S/m. Local superficial-scalp layer conductivity (σ_{SS}) was a function of local skin electric field (E_{SS}) given by:

$$\sigma_{SS} = (4.34e^{-4})E_{SS} - 0.0152 \qquad \text{(Equation 1)}$$

Where $\sigma_{\overline{SS}}$ is subject specific maximum superficial-scalp conductivity. We emphasize that $\sigma_{\overline{SS}}$ varies across the scalp surface such that σ_{SS} then varies across the head (higher near electrodes). For each subject two model parameters were individualized: deep-scalp layer conductivity (σ_{DS}) and maximum superficial-layer conductivity $\sigma_{\overline{SS}}$.
Stimulation electrodes and gels were modeled in SolidWorks (Dassault Systèmes Corp., Waltham, MA). We represented ECT adhesive pad electrodes with area of 4.2 by 4.9 cm and thickness of ~ 1.7 mm, and conductivity of 0.018 S/m (based on Thymapad electrodes), while the circular metal electrodes with a diameter of 5 cm and conductivity of 0.018 S/m.

Computation and subject specific tissue parameterization

These modeled electrodes and gels were incorporated into the segmentation. Volume meshes were generated from the segmented data and eventually exported to COMSOL Multiphysics 5.5 (COMSOL Inc., MA, USA). The resulting mesh comprised > 9,000,000 tetrahedral elements (>15,000,000 degrees of freedom).

We modeled two electrode configurations:

1. ‘Bifrontal pad electrode montage’: The center of the both electrodes are on a first imaginary line that starts at the lateral canthus and projects up parallel to the facial midline. The long edge of the electrodes is aligned parallel to the first imaginary line such that the short edge of the pad electrodes is approximately parallel to the horizontal plane. The short edge of the pad electrodes is right above supraorbital ridge (approximately above the eyebrow). Depending on the subject, the center of the electrodes ends up approximately 3-5 cm above the canthus of the eye.
2. ‘Right Unilateral (RUL) disk electrode montage’: The center of the frontotemporal disk electrode is aligned with the midpoint of an imaginary line between the tragus and lateral canthus of the eye. The bottom of the disk electrode is placed right above the imaginary line. The posterior edge of superior electrode disk is placed approximately ½-1 inch anterior to the vertex, which is the intersection of imaginary lines from nasion to inion, and the intertragal line.

The Laplace equation $\nabla . (\sigma \nabla V) = 0$ (V: scalar electric potential; ∇: gradient vector; σ: conductivity) was solved and the boundary conditions were used such as current in static models 1 mA and dynamic models 900 mA is applied to through one of the electrode terminals, while

the other electrode is grounded at both montage types in all subjects. Superficial skin conductivity was implanted as a function of electric field (equation 1). The finite element method (FEM) model was implemented using COMSOL. To converge the solution, a linear system solver of conjugate gradients was used with a relative tolerance of $1x10^{-3}$ with a nonlinear system solver using the Newton-Raphson method (<500 iterations). This method is applied to millions of degrees of freedom iteratively. Note non-adaptive approaches would require a single Newton-Raphson iteration requiring ~100-500 iteration of the conjugate gradient solver. The total iterations increase to ~ (2-10k) in the adaptive model involving ~ (60-100) Newton-Raphson iterations.

For each subject (#21908, #22615, #22035, #21778), experimentally reported static impedance and dynamic impedance were determined. Static impedances were averaged across the first non-titrated session of each visit while the dynamic impedances were averaged across every session specific to visits where seizure was generated. An iterative approach was used to search deep-scalp layer conductivity (σ_{DS}) and maximum superficial-layer conductivity ($\sigma_{\overline{SS}}$) until electric fields converged within the specified relative tolerance.

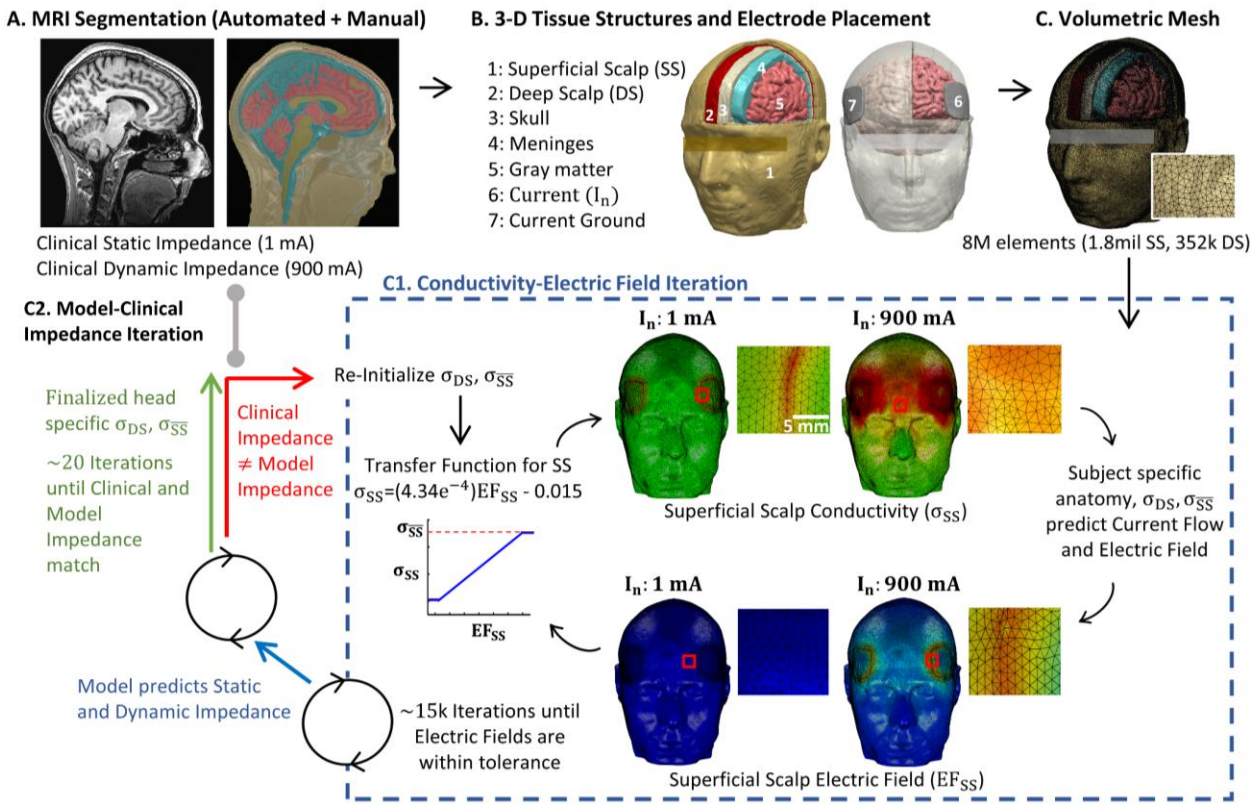

Figure 1. Novel adaptive computational pipeline for ECT current flow FEM models. We develop the first image-derived numerical models of transcranial electrical stimulation (tES) incorporating local changes in tissue conductivity in response to local current flow (electric fields). (A) T1-weighted anatomical MRIs were collected from ECT patients, with clinical static impedance and dynamic impedance data. (B) Volume conductor models were created preserving image resolution using methods previously developed for low-intensity tES [17] [23] [16] - however here we divide scalp into Superficial Scalp (SS) and Deep Scalp (DS) compartments. Skull, meninges, gray matter, and white matter compartments are assigned standard fixed tissue conductivities. Clinical electrode montages are reproduced (e.g. BF) with boundary conditions corresponding to static impedance (I_n = 1 mA) and

dynamic impedance (I_n=900 mA) testing. (C) For each subject and electrode montage, a volumetric mesh is generated from the segmented data. (D) The model is initialized with a deep scalp conductivity (σ_{DS}) and a maximum superficial scalp conductivity ($\sigma_{\overline{SS}}$). Independently for 1 mA and 900 mA current, an iterative model then computes current flow based on tissue resistivities, updates superficial scalp conductivity ($\sigma_{\overline{SS}}$) in each element based on local electric fields using a transfer function, and then recalculates brain current flow (blue dashed square). The model converges after ~15k iterations, producing a model prediction of static impedance (for 1 mA) and dynamic impedance (for 900 mA). (E) Model predicted static and dynamic impedance are compared with clinical static and dynamic impedance from the subject. If there is any significant mismatch, the model is reinitialized with updated deep scalp conductivity (σ_{DS}) and a maximum superficial scalp conductivity ($\sigma_{\overline{SS}}$), and the FEM is re-run until convergence (blue dashed square). When model static and dynamic impedance match clinical data, a patient specific deep scalp conductivity (σ_{DS}) and a maximum superficial scalp conductivity ($\sigma_{\overline{SS}}$) is set.

Results

ECT Stimulation Parameter Analysis from a Single Center Trial

While static impedance and dynamic impedance has long been recognized as markers of individual difference in electroconvulsive therapy (ECT), their etiology and consequence are undetermined – including how they impact seizure generation. A typically high static impedance is relied on to suggest an expected high dynamic impedance, and hence the need to correct electrode setup. Yet, the correlation between individual static impedance and dynamic impedance has remained elusive, with numerous prior studies suggesting it does not exist. This is a retrospective analysis of static impedance, dynamic impedance, seizure charge threshold, and patient demographic data recorded from a total of 90 patients (with a total of 622 ECT stimulations) involved in a previously published clinical trials.

ECT data comparing montage (RUL vs BL) and waveform (brief pulse vs ultra-brief pulse) was re-analyzed from a single-center trial [24] – importantly for our purposes here, other stimulation protocols parameters were reliably controlled and fixed (e.g. device, electrodes, operator experience, preparation technique). Across ECT conditions, dynamic impedance increases with static impedance (Fig 2) with significant interactions both across subjects within ECT condition and within subject across repeated sessions (not shown).

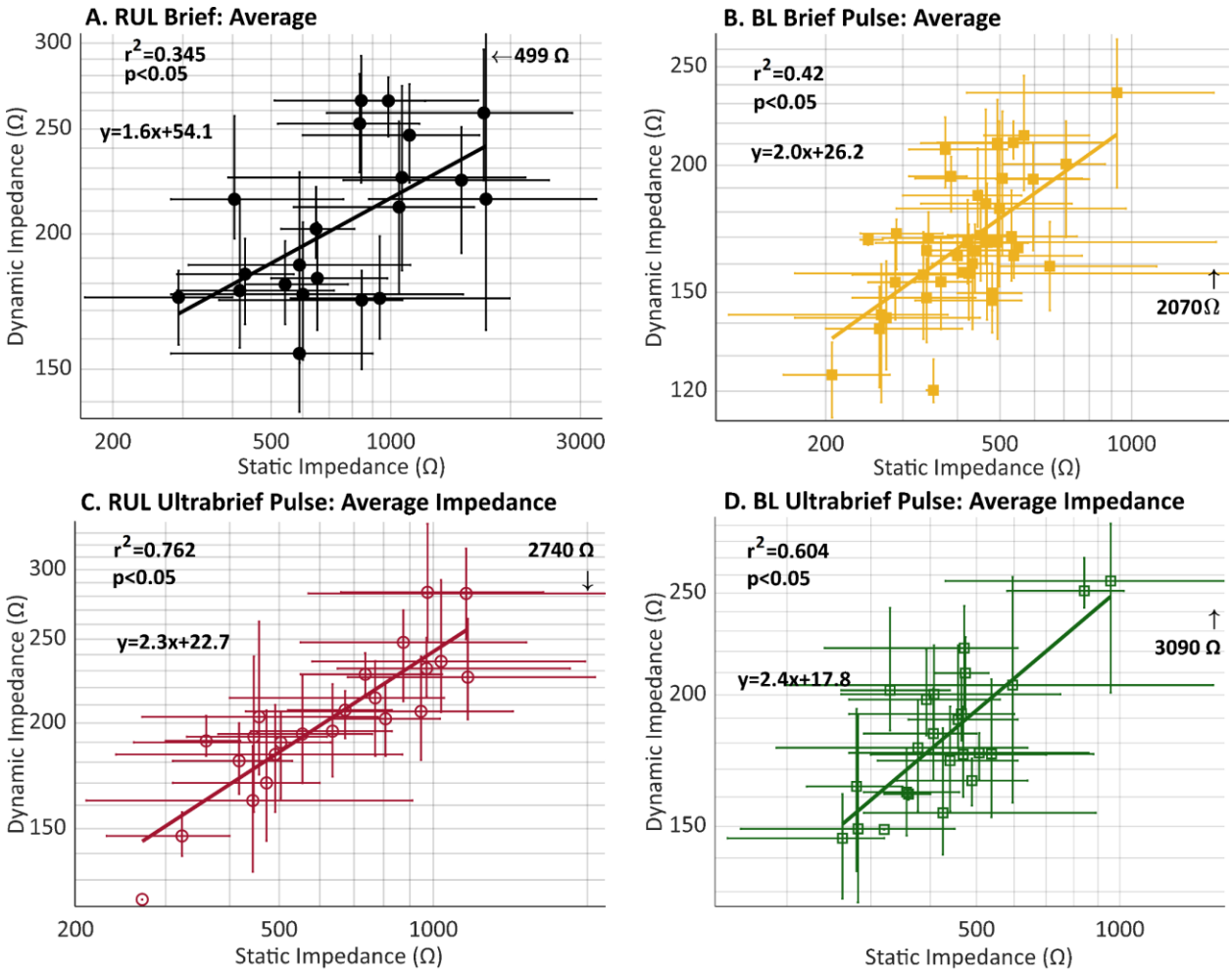

Figure 2. Retrospective analysis of data from a single center ECT trial comparing RUL and BL montages and Brief and Ultra-Brief pulse durations. Across (A) RUL Brief Pulse (black), (B) BL Brief Pulse (yellow), (C) RUL Ultrabrief Pulse (red), and BL Ultrabrief pulse (green) there was a significant correlation between subject static impedance and dynamic impedance. The average impedance across sessions is represented for each subject as well as the full range of variance (error bars).

Impact of electrode preparation on static impedance

In a sample of healthy subject, we measured static impedance systematically varying adhesive electrode preparation technique repeated (Fig. 3). All electrode preparation conditions using an adhesive (Pretac or PVP-K90) resulted in a comparable and minimal static impedance for each given subject, with no significant effect of application time. Absence of adhesive (alcohol skin cleaning only) increased static impedance. Reduction in electrode contact area by 50% increased static impedance a factor of ~1.7x. Excluding conditions of limited electrode-skin contact, the lower static impedance reported by Mecta device compared Thymatron device did not impact rank order or reliability.

Even under our tightly controlled experimental conditions and with optimal preparation (use of adhesive), moderate variability was observed between repetition trials. Under realistic clinical conditions, variability both in the quantity (area coverage) and quality (e.g. adhesion) of

electrodes could produce substantial impedance variance. Nevertheless, it is important for our modeling efforts that, assuming good ECT electrode preparation, difference between individuals are not dominated by idiosyncrasy in the quality of electrode-skin contact (i.e. as models assume complete electrode-skin contact) but rather reflects subject's head properties.

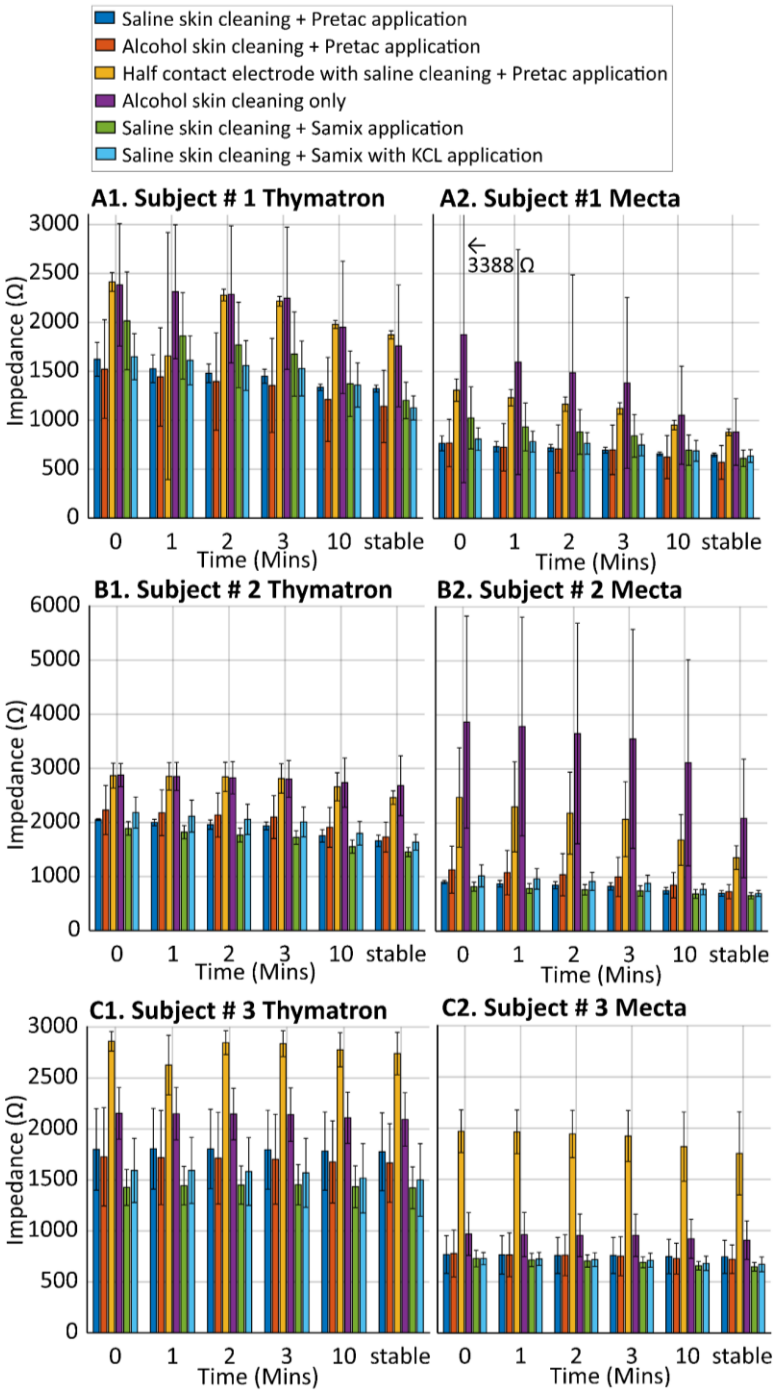

Figure 3: Static impedance over time under six electrode preparations. Each condition measured at least three times on the Thymatron (1) and Mecta (2) devices in subject 1 (A), subject 2 (B), and subject 3 (C).

Development of Individualized Adaptive Tissue Models of ECT

MRI-derived head models to address differences in resulting brain current flow were developed [17,25] and validated [26,27] for low-intensity transcranial electrical stimulation, and then applied to ECT [12,28]- all under assumption of non-adaptive tissue resistivity. Here we apply our novel pipeline for adaptive tissue conductivity (where local conductivity changes with electric field) to ECT (Fig. 4). The analysis is applied to data from for ECT patients. For each patient anatomical MRI as segmented and an iterative search process identifies the maximum superficial skin conductivity ($\sigma_{\overline{SS}}$) and the deep skin conductivity (σ_{DS}) that produces prediction of static and dynamic impedance corresponding to subject clinical data.

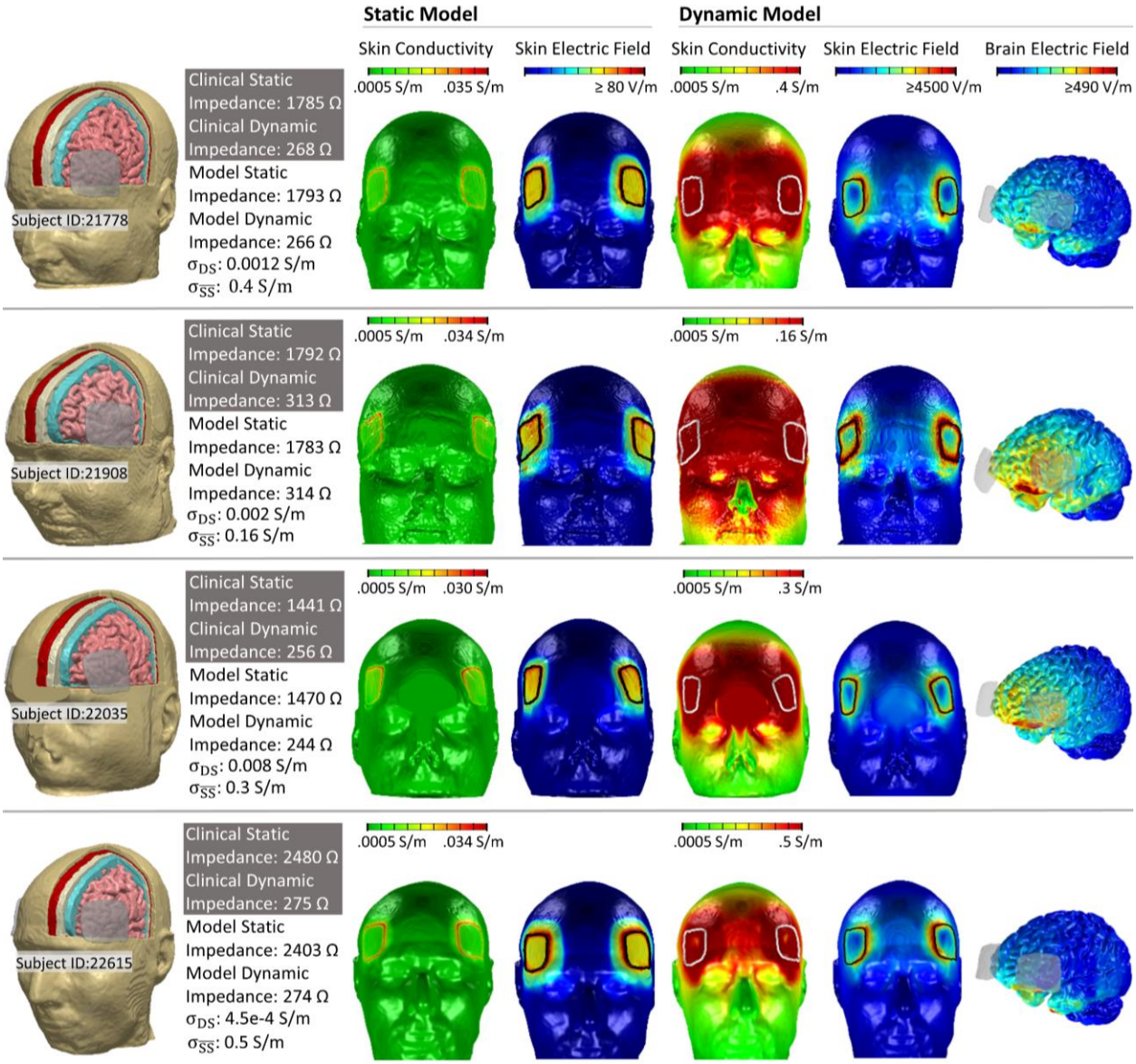

Figure 4. Dynamic ECT models for four ECT patients. Dynamic FEM models simulated current flow across four subjects who have received ECT (Subject IDs: 21778, 21908. 22035, 22615). (First Column) Models anatomy was based in subject anatomical MRI. Clinical static impedance and dynamic impedance were recorded for each subject

(grey box). Each subject model was assigned a specific deep scalp conductivity (σ_{DS}) and a maximum superficial scalp conductivity ($\sigma_{\overline{SS}}$) as indicated, such that adaptive FEM simulation predicted corresponding static impedance (based on 1 mA applied current) and dynamic impedance (based on 900 mA applied current) as indicated. (Second and Third Column) Results from the static impedance (1 mA current) simulation showing resulting superficial skin conductivity and skin electric field. (Third, Fourth, Fifth Column) Results from the dynamic impedance (900 mA current) simulation showing resulting superficial skin conductivity, skin electric field, and brain electric field. We emphasize in these novel adaptive simulations, that brain current flow was determined by tissue conductivity, superficial skin conductivity was simultaneously determined by local electric field. Even for the 1 mA (static) model local changes in skin conductivity are predicted. For the 900 mA (dynamic) model, the saturation of the transfer function between superficial skin electric field and conductivity results in a more diffuse saturation of skin conductivity (front of head) compared to skin electric field (around electrodes.

Adaptive skin response and the relation between static and dynamic impedance

The role of head anatomy in ECT outcomes remains unclear, and is complex to understand experimentally when gross anatomy, tissue properties, and neurophysiology all vary. The role of gross anatomy can be considered using computational models by 1) fixing head anatomy by manipulating tissue (skin) properties; or 2) artificially changing (e.g. dilating) anatomy in a single head. These approaches are used first to explain the relation between dynamic and static impedance, and then how these impact delivery of intensity current of the brain.

Given the optimized deep-layer skin conductivity (σ_{DS}) and maximum superficial-layer conductivity ($\sigma_{\overline{SS}}$) for each head, it is possible to consider the role of skin properties by simulating swapping skin properties anatomical head. (Fig. 5). Starting from a base set of four head anatomies (Subject 22615, square; Subject 21778, diamond; Subject 22035, circle; Subject 21908, x with corresponding (σ_{DS}) and () for each subject, we then swapped (mixed) skin properties across heads (colors), resulting in 12 synthesized heads (plus the 4 originals). Under an assumption that a hypothetical subjects head anatomy, deep-layer skin conductivity (σ_{DS}) and maximum superficial-layer conductivity ($\sigma_{\overline{SS}}$) can vary independently each synthesized head represent a hypothetical subject. In any case, this approach allows systematic comparison of the relative impact of anatomy and skin properties to ECT outcomes as predicted by the synthetic models.

This relationship between static impedance and dynamic impedance is evident though weak in the corresponding clinical data (Fig. 5 A). The relationship between static impedance and dynamic impedance across the synthetic heads is not evident across swapped head models (Fig 5 B) though interactions are evident when considering individual head anatomy (Fig. 5 B1, B2, B3, ,B4).

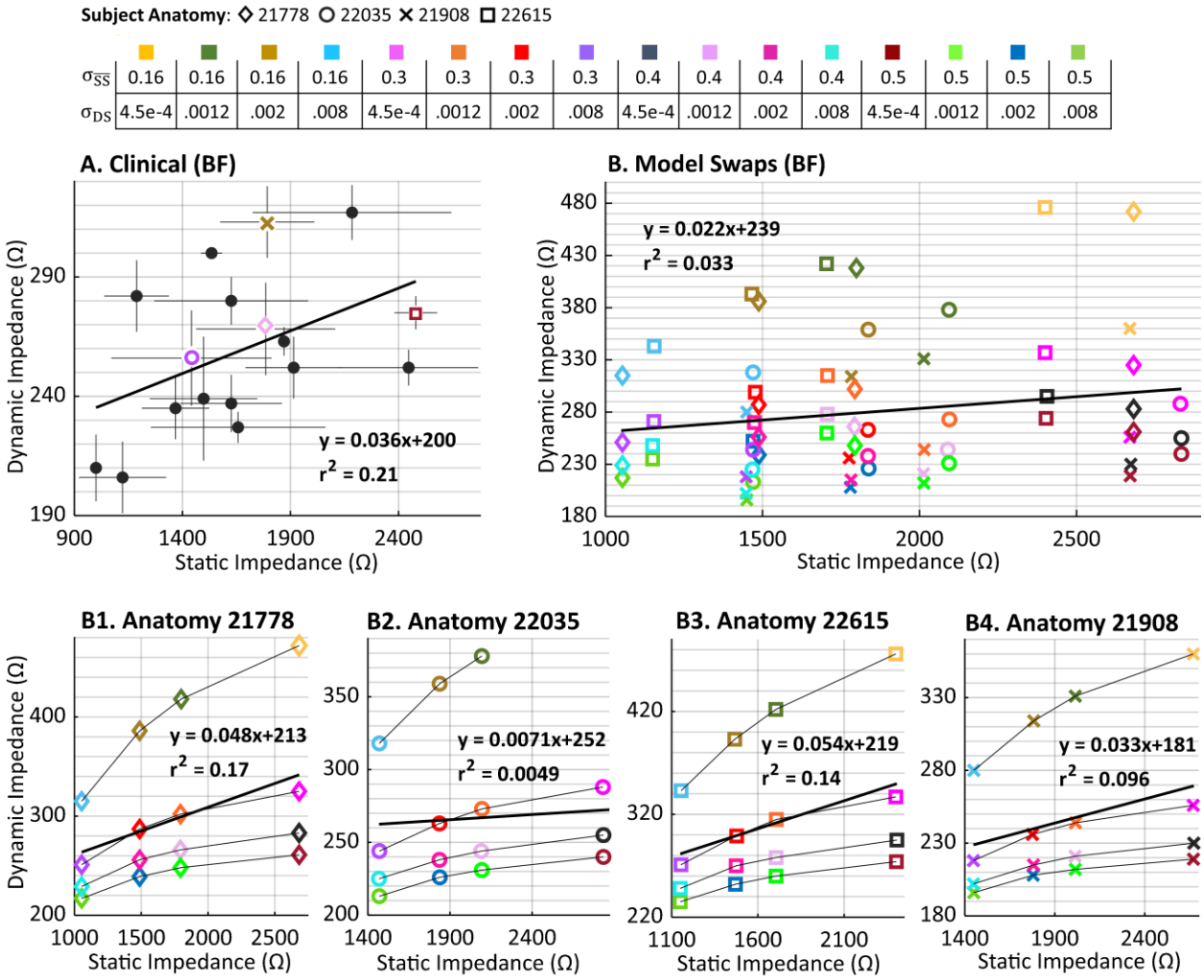

Figure 5. Relation between Dynamic Impedance and Static Impedance in clinical data and adaptive models including skin swaps. (A) Dynamic impedance and static impedance were weakly correlated in an exemplary patient sample receiving BF ECT. Four subjects (colored symbols) were selected for adaptive FEM simulation. (B) In these four subjects, clinical static and dynamic impedance were simulated by assigning subject specific deep scalp conductivity (σ_{DS}) and a maximum superficial scalp conductivity ($\sigma_{\overline{SS}}$). The conductivities (in S/m) are called "endogenous" for our purposes here (Subject 22035 σ_{DS}= 0.008, $\sigma_{\overline{SS}}$= 0.3; Subject 21778 σ_{DS}= 0.0012, $\sigma_{\overline{SS}}$= 0.4; Subject 21908 σ_{DS}= 0.002, $\sigma_{\overline{SS}}$= 0.16; Subject 22615 σ_{DS}= 4.5e^{-4}, $\sigma_{\overline{SS}}$= 0.5). In scalp swaps, all deep scalp conductivity (σ_{DS}) and a maximum superficial scalp conductivity ($\sigma_{\overline{SS}}$) were varied across all subject anatomies, resulting in 16 simulates swapped-conductivity heads (including the endogenous 4 heads). For each head, static impedance and dynamic impedance was predicted using our adaptive pipeline. There is only a weak correlation between simulated static and dynamic impedances. (B1, B2, B3, B4) Replotting the same points but separated by subjects, highlights certain trends. For a given head anatomy and a given deep scalp conductivity (σ_{DS}), varying superficial scalp conductivity ($\sigma_{\overline{SS}}$) changes dynamic impedance but not static impedance. This vertical distribution of dynamic impedances for a given static impedance reduces overall correlation across all simulations, but even within a single anatomy. For a given head anatomy and superficial scalp conductivity ($\sigma_{\overline{SS}}$), decreasing superficial scalp conductivity ($\sigma_{\overline{SS}}$) monotonically increases both static impedance and dynamic impedances, explaining the source of overall (weak) correlation.

Variation in skin properties are relatively more important than gross anatomy in governing static impedance and dynamic impedance. Specifically, extreme variations in static impedance and dynamic impedance are governed by $\sigma_{\overline{SS}}$ and σ_{DS} respectively. Therefore, because $\sigma_{\overline{SS}}$ and σ_{DS} vary independently a dispersion of static and dynamic conductivities is produced. A weak interaction persists because σ_{DS} has (in addition to a strong effect on static impedance) a weak effect on dynamic impedance. Head anatomy does moderate both static and dynamic impedance (see also below). The importance of deep-layer skin (σ_{DS}) conductance, with head anatomy as a moderator, on static impedance is evident when noting that for a given head and σ_{DS} conductance static conductivity is nearly fixed, despite variation in dynamic impedance. This vertical dispersion is also why a relationship between static and dynamic impedance is not evident (e.g. for static impedance >2600 a range of dynamic impedance is possible)

Across (almost all) the variety of adaptive-tissue properties, the rank order of dynamic impedance was fixed (from higher to lowest: Subject 22615, square; Subject 21778, diamond; Subject 22035, circle; Subject 21908, cross). Across variation in adaptive-tissue properties, the rank order of static impedance was not consistent across heads, though some trends were evident. Subject 22035 present the highest relative static impedance. Subject 22615 present the lowest relative static impedance. Neither rank order for static impedance or dynamic impedance corresponded to the rank order of any global anatomical parameter, suggested it is not possible to predict (relative) static or dynamic impedance based on any simple anatomical measure (consistent with clinical observations).

The result here is not that the modeling approach cannot match the clinical data, since evidently adjusting each subject $\sigma_{\overline{SS}}$ and σ_{DS}. Fig. 4 could ensure perfect model approximation of the clinical data. Rather, the mismatch between the swapped skin property synthetic heads and clinical data a correlation between static and dynamic impedance suggesting either 1) there is a stronger co-moderator (σ_{DS}) 2) factor not modeled (e.g. a different adaptive model or a experimental feature such as electrode coverage).

Adaptive skin response and the relation between brain current intensity and static or dynamic impedance

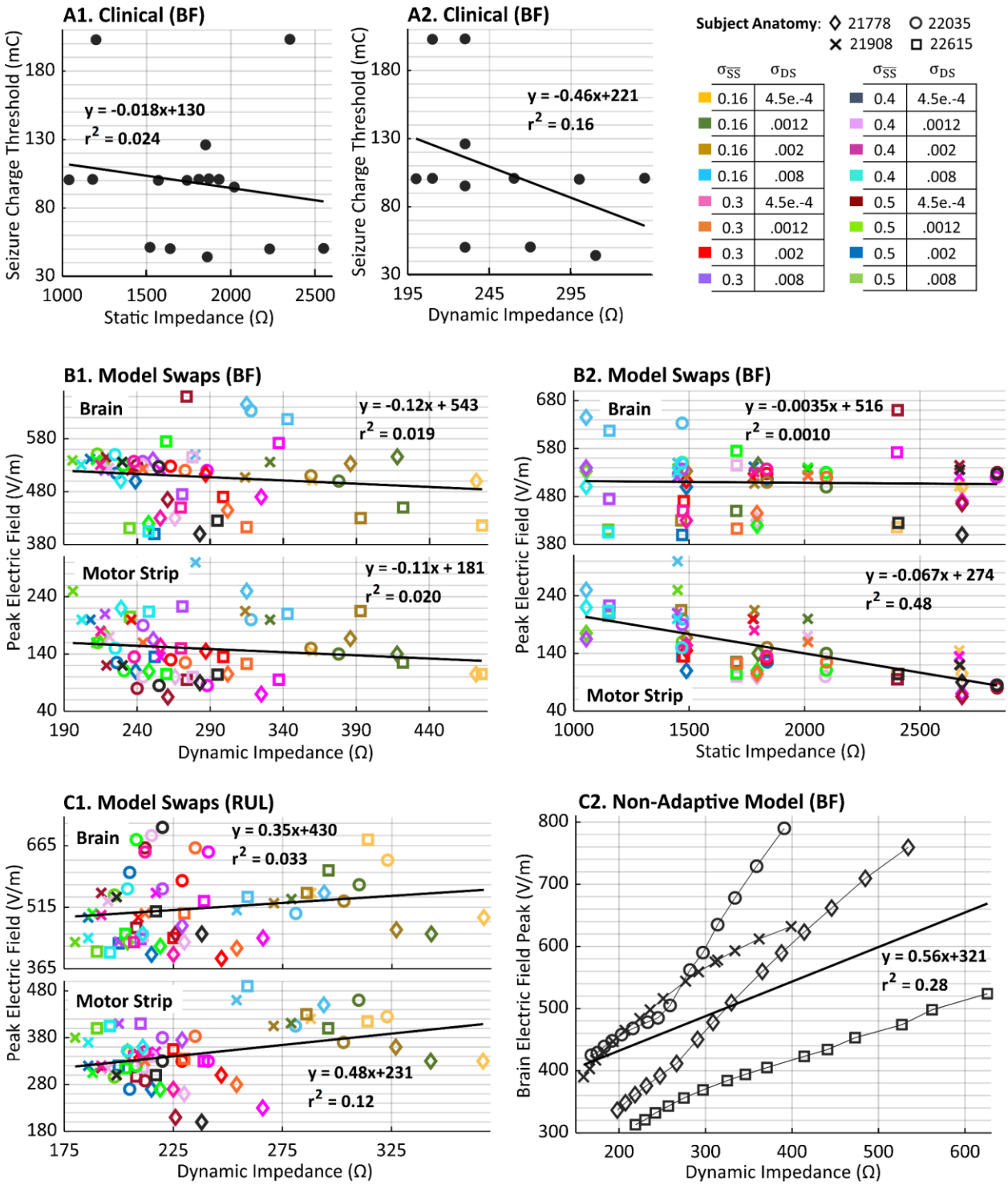

Figure 6. Relation between brain Electric field (or seizure charge threshold) in clinical data and adaptive skin models including skin swaps. In theory, conditions that result is higher electric fields (at the region of seizure initiation) will be associated with reduces charge threshold to trigger a seizure. (A) In an exemplary patient sample receiving BF ECT, there was a very weak relation between increasing static impedance (A1) or increasing dynamic impedance (A2) and decreasing charge threshold for seizure initiation. (B) The predicted relation between brain electric field and dynamic impedance (B1) or static impedance (B2) can be simulated for the BF electrode montage using adaptive FEM models of the 16 swapped-conductivity heads (including the endogenous 4 heads). Brain wide

peak electric field is considered (higher panel) as well as motor strip peak electric field (lower panel). Only weak correlations are predicted, with the strongest correlation (negative direction) for the case of static impedance and motor strip peak electric fields. (C1) Using adaptive FEM modeling, the relation between dynamic impedance and static impedance was further predicted in same heads for the RUL electrode montage. Weak correlation was predicted, with the strongest correlation (positive direction) for dynamic impedance and motor strip peak electric field. (C2) Non- conventional FEM of the four anatomical head, where for each uniform scalp conductivity was varied to adjust dynamic impedance, predicted quasi-linear relationship for each head between dynamic impedance and brain electric field. Variability between heads resulted in a weaker group correlation between dynamic impedance and brain electric field. We note the prediction in non-adaptive conventional stimulation of increasing electric field with increased dynamic impedance is expected and consistent with scalp resistivity increasing both. The predictions from adaptive FEM suggest a more complex and nuanced relationship between dynamic impedance and electric field (and so charge needed to produce seizures).

In the corresponding BF ECT clinical data, there was no evident relation between static impedance and seizure charge threshold or dynamic impedance and seizure charge threshold. Across the swapped BF head model stimulation, we predicted peak electric fields, both brain wide and specifically in the motor strip. There was no evident correlation between static or dynamic impedance, and brain peak electric field or motor strip electric field. The exception between a weak native relation between static impedance and motor strip peak electric field.

While these adaptive models were parametrized based on BF ECT data, we used the same swapped heads to predict for RUL ECT the relation between static impedance or dynamic impedance and brain current delivery (Fig. 6 C1). Relationships were weak, and trended positive. We further considered non-adaptive models in order to highlight the unique behavior of adaptive models (Fig 6 C2). In non-adaptive models, for each subject head the uniform skin conductivity is incrementally decreases, produced a range of impedance (there is no sense of distinguished static or dynamin impedance in these cases). As expected, brain electric field increased monotonically for reach subject with increased impedance. This slope varies across heads but remains significant across the group.

MRI-derived head models can be artificially altered [29] including dilation of specific tissue layers [18,23]. Keeping tissue conductivity properties fixed (as optimized for each subject), we first dilated only superficial-layer skin by ~6x (Fig 7). Superficial-skin dilation increased static impedance (Subject 22615, 2403 ohm to 2931 ohm; Subject 21778, 1793 ohm to 2428 ohm; Subject 21908, 1783 ohm to 2450 ohm), decreased dynamic impedance (Subject 22615, 274 ohm to 206 ohm; Subject 21778, 266 ohm to 199 ohm; Subject 21908, 314 ohm to 262 ohm), and decreased current delivery (Subject 22615, 660 V/m to 411 V/m peak, 95 V/m to 68 V/m motor cortex; Subject 21778, 460 V/m to 320 V/m peak, 115 V/m to 85 V/m motor cortex; Subject 21908, 507 V/m to 438 V/m peak, 215 V/m to 150 V/m motor cortex). Further dilation deep skin layer by ~2x increased static impedance (Subject 22615, 2403 ohm to 3819 ohm; Subject 21778, 1793 ohm to 2944 ohm; Subject 21908, 1783 ohm to 2740 ohm), decreased dynamic impedance (Subject 22615, 274 ohm to 219 ohm; Subject 21778, 266 ohm to 217 ohm; Subject 21908, 314 ohm to 295 ohm), and decreased current delivery (Subject 22615, 660 V/m to 463 V/m peak, 95 V/m to 64 V/m motor cortex; Subject 21778, 460 V/m to 300 V/m peak, 115 V/m to 70 V/m motor cortex; Subject 21908, 507 V/m to 413 V/m peak, 215 V/m to 120 V/m motor cortex). Notably, these simulations show a dissociation of static impedance, dynamic impedance, and electric field in the sense specific intervention can affect them relatively differently. This also reinforces the unique outcomes, and so value, of adaptive-resistivity models.

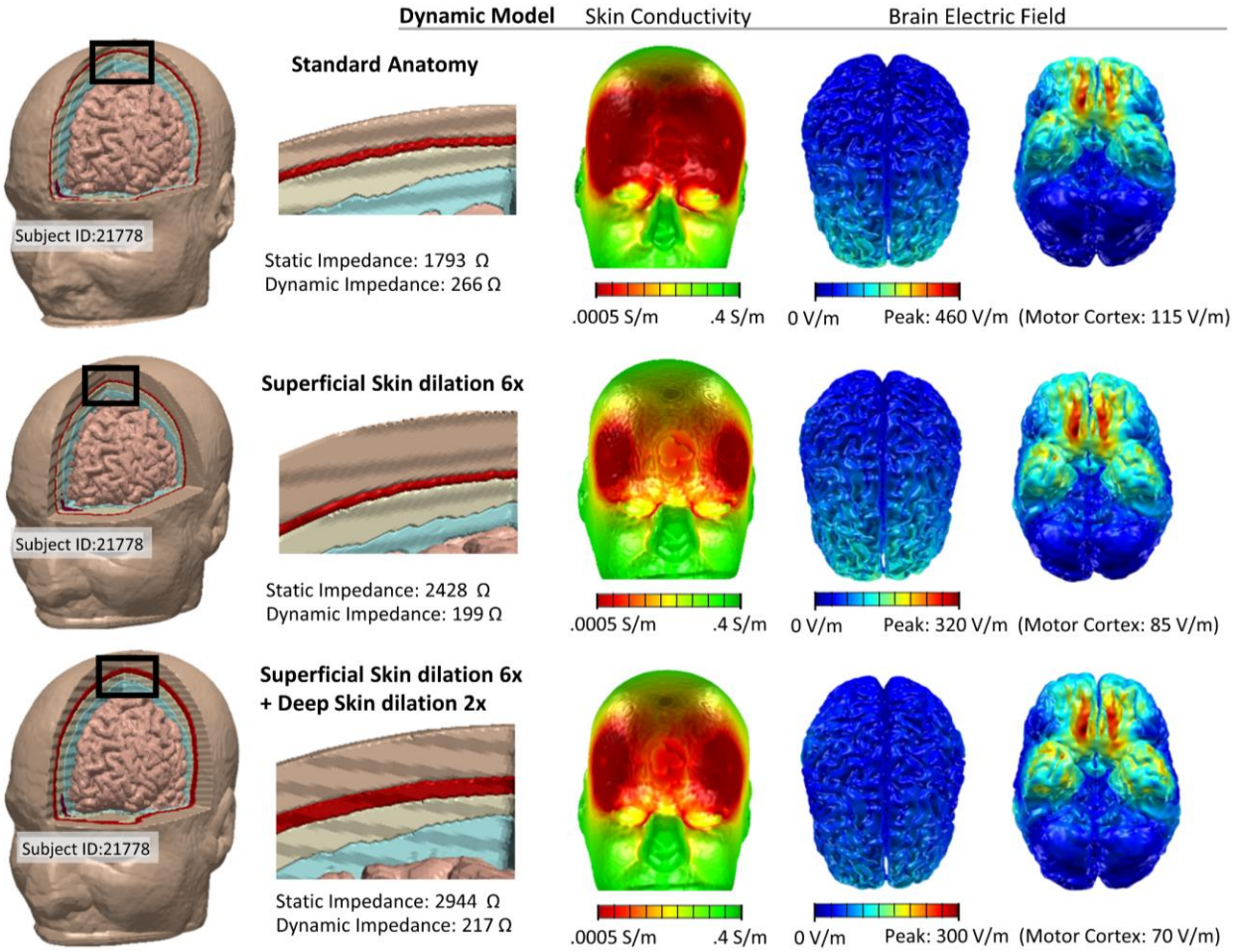

Figure 7: **Tissue Dilation in Adaptive FEM model of ECT, and relationship between static impedance, dynamic impedance, and brain electric field.** Our adaptive FEM models suggest a complex relationship between head anatomy, tissue properties, and resulting current flow and resistance. In addition to allowing variance of just select tissue conductivity, computational models can access the role of isolated anatomy, including through superficial tissue dilation [18]. We considered standard (original) anatomy (top row), dilating superficial scalp 6-fold (middle row), and further dilating deep scalp 2-fold (bottom row). In the last case, dilated deep scalp replaces overlying superficial scalp. Compared to the standard anatomy, dilating superficial scalp 6-fold increased static impedance, decreased dynamic impedance, and decreased brain electric field. Further dilating deep scalp 2-fold, increase static impedance, increase dynamic impedance, and decreased further brain electric field. These adaptive FEM simulations show a subtle non-monotonic relationship between static impedance, dynamic impedance, and brain electric fields.

Response to moderated ECT Voltage and Current: Model validation against classical clinical data

While conventional ECT used currents of ~900 mA, in two earlier trials the current and/or voltage of ECT was systematically reduced within subjects, which can be replicated in simulations (Fig. 8). Dynamic impedance as a function of voltage from Umlauf et al. 1951 and Maxwell et al. 1968, and dynamic impedance as a function of current for Umlauf et al. 1951 are replotted for each individual subject (grey lines) and group average (yellow Maxwell et al. 1968; black Umlauf et al. 1951) which are fit by a power law:

$R = a(V^b)$ (Equation 2)
$R = a(I^b)$ (Equation 3)

Where R is Dynamic Impedance (in Ohms), V is voltage applied (in Volts), I is current applied (in mA) and a and b are constants.
Alongside clinical experimental data, results from reducing the applied voltage and current in out adaptive-conductivity models heads is shown and also fit to power law. The models generally reproduce the power law relationship, with individual difference (in a,b). Absolute matching of parameters (a,b) is not expected given different in protocol; including Umlauf et al. 1951 and Maxwell et al. 1968 used sinusoidal and our models were train line on pulse trains; it is known dynamic impedance is relatively higher for pulse compared to sinusoid.

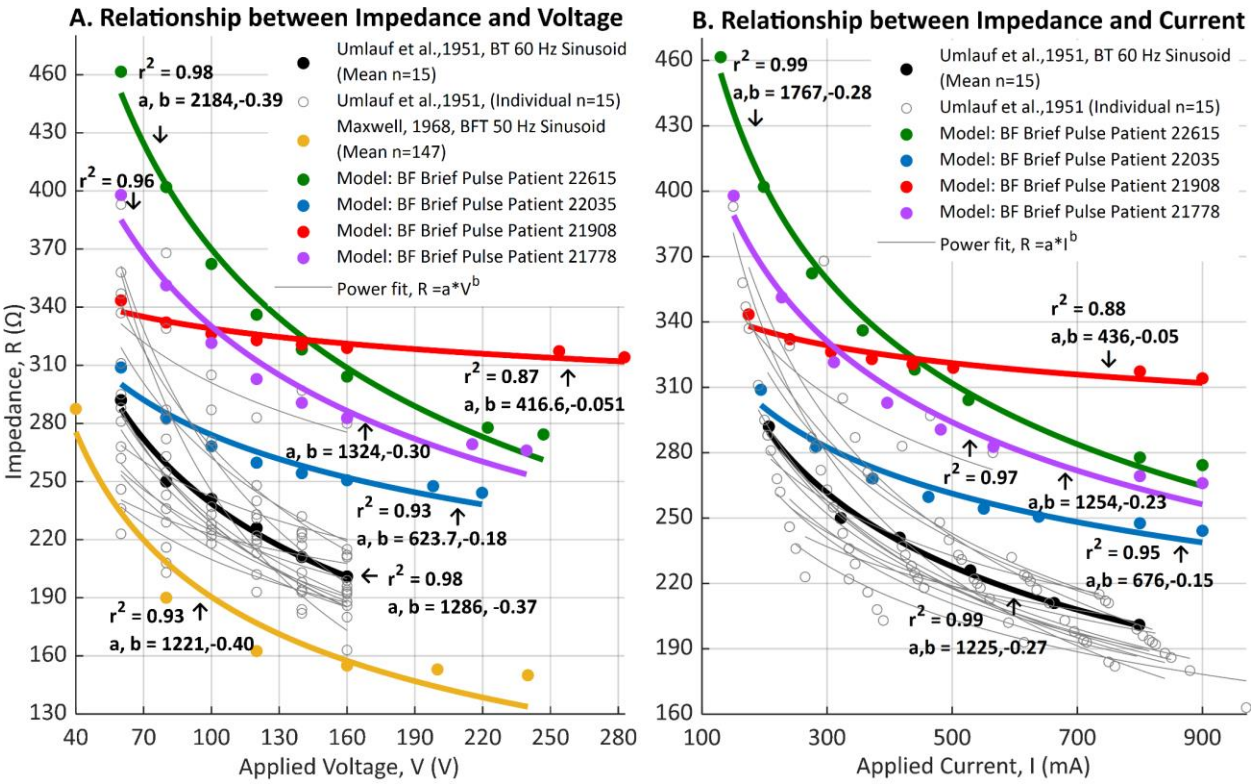

Figure 8: Relationship between reduced applied ECT voltage or current and Dynamic Impedance, clinical and modeling results. While in conventional ECT the current level if fixed, in historical experiments the current and/or the voltage was reduced while monitoring dynamic impedance. In Umlauf et al. (1951), the intensity of ECT (using 60 Hz sinusoidal waveforms, BT electrode montage) was decreased, with resulting impedance reported as a function of both applied voltage (A) and applied current (B) [5]. Individual subject data (grey) is reported, alongside group average (black). In Maxwell et al. (1968), the voltage of ECT (using 50 Hz sinusoidal waveform, BFT electrode montage) was reported against dynamic impedance (group average only, yellow)[13]. Using adaptive FEM, for each head (Subject IDs: 21778, 21908, 22035, 22615), we systematically varied the current intensity applied to dynamic impedance of the model and simulated the resulting dynamic impedance (B) while also reported the associated voltage (A). Our models were parameterized based on pulsed waveforms (only for 1 mA and 900 mA). Average clinical data and individual model data were fit by a power law. While absolute difference between

clinical cases and models are expected (e.g. given variation in protocol and the dependence of conductivity on waveform), the power law well fits clinical and modeling data.

REFERENCES:

[1] Peterchev AV, Rosa MA, Deng Z-D, Prudic J, Lisanby SH. Electroconvulsive therapy stimulus parameters: rethinking dosage. J ECT 2010;26:159–74. https://doi.org/10.1097/YCT.0b013e3181e48165.

[2] Peterchev AV, Wagner TA, Miranda PC, Nitsche MA, Paulus W, Lisanby SH, et al. Fundamentals of Transcranial Electric and Magnetic Stimulation Dose: Definition, Selection, and Reporting Practices. Brain Stimul 2012;5:435–53. https://doi.org/10.1016/j.brs.2011.10.001.

[3] Sackeim HA, Prudic J, Devanand DP, Nobler MS, Lisanby SH, Peyser S, et al. A prospective, randomized, double-blind comparison of bilateral and right unilateral electroconvulsive therapy at different stimulus intensities. Arch Gen Psychiatry 2000;57:425–34. https://doi.org/10.1001/archpsyc.57.5.425.

[4] Weiner RD, Rogers HJ, Davidson JR, Squire LR. Effects of stimulus parameters on cognitive side effects. Ann N Y Acad Sci 1986;462:315–25. https://doi.org/10.1111/j.1749-6632.1986.tb51266.x.

[5] Umlauf CW, Gunter RC, Tunnicliffe WW. Impedance of the human head as observed during electro-shock treatment. Confin Neurol 1951;11:129–38. https://doi.org/10.1159/000105632.

[6] Delva NJ, Brunet D, Hawken ER, Kesteven RM, Lawson JS, Lywood DW, et al. Electrical dose and seizure threshold: relations to clinical outcome and cognitive effects in bifrontal, bitemporal, and right unilateral ECT. J ECT 2000;16:361–9. https://doi.org/10.1097/00124509-200012000-00006.

[7] Chung KF, Wong SJ. Stimulus dose titration for electroconvulsive therapy. Psychiatry Clin Neurosci 2001;55:105–10. https://doi.org/10.1046/j.1440-1819.2001.00795.x.

[8] Coffey CE, Lucke J, Weiner RD, Krystal AD, Aque M. Seizure threshold in electroconvulsive therapy (ECT) II. The anticonvulsant effect of ECT. Biol Psychiatry 1995;37:777–88. https://doi.org/10.1016/0006-3223(95)00053-J.

[9] van Waarde JA, van Oudheusden LJB, Verwey B, Giltay EJ, van der Mast RC. Clinical predictors of seizure threshold in electroconvulsive therapy: a prospective study. Eur Arch Psychiatry Clin Neurosci 2013;263:167–75. https://doi.org/10.1007/s00406-012-0342-7.

[10] Sackeim HA, Long J, Luber B, Moeller JR, Prohovnik I, Devanand DP, et al. Physical properties and quantification of the ECT stimulus: I. Basic principles. Convuls Ther 1994;10:93–123.

[11] Lee WH, Deng Z-D, Kim T-S, Laine AF, Lisanby SH, Peterchev AV. Regional electric field induced by electroconvulsive therapy: a finite element simulation study. Conf Proc IEEE Eng Med Biol Soc 2010;2010:2045–8. https://doi.org/10.1109/IEMBS.2010.5626553.

[12] Bai S, Gálvez V, Dokos S, Martin D, Bikson M, Loo C. Computational models of Bitemporal, Bifrontal and Right Unilateral ECT predict differential stimulation of brain regions associated with efficacy and cognitive side effects. Eur Psychiatry 2017;41:21–9. https://doi.org/10.1016/j.eurpsy.2016.09.005.

[13] Maxwell RDH. Electrical Factors in Electroconvulsive Therapy. Acta Psychiatrica Scandinavica 1968;44:436–48. https://doi.org/10.1111/j.1600-0447.1968.tb07648.x.
[14] Gomez-Tames J, Sugiyama Y, Laakso I, Tanaka S, Koyama S, Sadato N, et al. Effect of microscopic modeling of skin in electrical and thermal analysis of transcranial direct current stimulation. Phys Med Biol 2016;61:8825–38. https://doi.org/10.1088/1361-6560/61/24/8825.
[15] Yamamoto T, Yamamoto Y. [Electrical properties of the epidermal stratum corneum]. Iyodenshi To Seitai Kogaku 1973;11:337–43.
[16] Jiang J, Truong DQ, Esmaeilpour Z, Huang Y, Badran BW, Bikson M. Enhanced tES and tDCS computational models by meninges emulation. J Neural Eng 2020;17:016027. https://doi.org/10.1088/1741-2552/ab549d.
[17] Datta A, Bansal V, Diaz J, Patel J, Reato D, Bikson M. Gyri-precise head model of transcranial direct current stimulation: improved spatial focality using a ring electrode versus conventional rectangular pad. Brain Stimul 2009;2:201–7, 207.e1.
[18] Truong DQ, Magerowski G, Blackburn GL, Bikson M, Alonso-Alonso M. Computational modeling of transcranial direct current stimulation (tDCS) in obesity: Impact of head fat and dose guidelines. NeuroImage: Clinical 2013;2:759–66. https://doi.org/10.1016/j.nicl.2013.05.011.
[19] Russell RW, Pierce JF, Townsend JC. Characteristics of tissue impedance in the rat under conditions of electroconvulsive shock stimulation. Am J Physiol 1949;156:317–21. https://doi.org/10.1152/ajplegacy.1949.156.3.317.
[20] Electrical Properties of Tissues in Shock Therapy - Franklin Offner, 1942 n.d. https://journals.sagepub.com/doi/abs/10.3181/00379727-49-13633?journalCode=ebma (accessed November 8, 2020).
[21] Ashburner J, Friston KJ. Unified segmentation. Neuroimage 2005;26:839–51. https://doi.org/10.1016/j.neuroimage.2005.02.018.
[22] Huang Y, Dmochowski JP, Su Y, Datta A, Rorden C, Parra LC. Automated MRI segmentation for individualized modeling of current flow in the human head. J Neural Eng 2013;10:066004. https://doi.org/10.1088/1741-2560/10/6/066004.
[23] Truong DQ, Magerowski G, Pascual-Leone A, Alonso-Alonso M, Bikson M. Finite Element study of skin and fat delineation in an obese subject for transcranial Direct Current Stimulation. 2012 Annual International Conference of the IEEE Engineering in Medicine and Biology Society (EMBC), 2012, p. 6587–90. https://doi.org/10.1109/EMBC.2012.6347504.
[24] Sackeim HA, Prudic J, Nobler MS, Fitzsimons L, Lisanby SH, Payne N, et al. Effects of pulse width and electrode placement on the efficacy and cognitive effects of electroconvulsive therapy. Brain Stimul 2008;1:71–83. https://doi.org/10.1016/j.brs.2008.03.001.
[25] Datta A, Truong D, Minhas P, Parra LC, Bikson M. Inter-Individual Variation during Transcranial Direct Current Stimulation and Normalization of Dose Using MRI-Derived Computational Models. Front Psychiatry 2012;3:91. https://doi.org/10.3389/fpsyt.2012.00091.
[26] Edwards D, Cortes M, Datta A, Minhas P, Wassermann EM, Bikson M. Physiological and modeling evidence for focal transcranial electrical brain stimulation in humans: A basis for high-definition tDCS. NeuroImage 2013;74:266–75. https://doi.org/10.1016/j.neuroimage.2013.01.042.

[27] Huang Y, Liu AA, Lafon B, Friedman D, Dayan M, Wang X, et al. Measurements and models of electric fields in the in vivo human brain during transcranial electric stimulation. Elife 2017;6. https://doi.org/10.7554/eLife.18834.
[28] Argyelan M, Oltedal L, Deng Z-D, Wade B, Bikson M, Joanlanne A, et al. Electric field causes volumetric changes in the human brain. Elife 2019;8. https://doi.org/10.7554/eLife.49115.
[29] Datta A, Bikson M, Fregni F. Transcranial direct current stimulation in patients with skull defects and skull plates: high-resolution computational FEM study of factors altering cortical current flow. Neuroimage 2010;52:1268–78.
[30] Fleming GWTH, Golla FL, Walter WG. ELECTRIC-CONVULSION THERAPY OF SCHIZOPHRENIA. The Lancet 1939;234:1353–5. https://doi.org/10.1016/S0140-6736(00)73899-2.
[31] Golla F, Walter WG, Fleming GW. Electrically Induced Convulsions: (Section of Psychiatry). Proc R Soc Med 1940;33:261–7.